Process Biochemistry 47 (2012) 1335–1343

Contents lists available at SciVerse ScienceDirect

Process Biochemistry

journal homepage: www.elsevier.com/locate/procbio

Use of *Spirulina platensis* micro and nanoparticles for the removal synthetic dyes from aqueous solutions by biosorption

G.L. Dotto, T.R.S. Cadaval, L.A.A. Pinto*

Unit Operation Laboratory, School of Chemistry and Food, Federal University of Rio Grande – FURG, 475 Engenheiro Alfredo Huch Street, 96203-900, Rio Grande, RS, Brazil

ARTICLE INFO

Article history:
Received 22 December 2011
Received in revised form 14 April 2012
Accepted 28 April 2012
Available online 7 May 2012

Keywords:
Acid blue 9
Biomass
Biosorption nature
FD&C red no. 40
Kinetics

ABSTRACT

In this research, micro and nanoparticles of *Spirulina platensis* dead biomass were obtained, characterized and employed to removal FD&C red no. 40 and acid blue 9 synthetic dyes from aqueous solutions. The effects of particle size (micro and nano) and biosorbent dosage (from 50 to 750 mg) were studied. Pseudo-first order, pseudo-second order and Elovich models were used to evaluate the biosorption kinetics. The biosorption nature was verified using energy dispersive X-ray spectroscopy (EDS). The best results for both dyes were found using 250 mg of nanoparticles, in these conditions, the biosorption capacities were 295 mg g^{-1} and 1450 mg g^{-1}, and the percentages of dye removal were 15.0 and 72.5% for the FD&C red no. 40 and acid blue 9, respectively. Pseudo-first order model was the more adequate to represent the biosorption of both dyes onto microparticles, and Elovich model was more appropriate to the biosorption onto nanoparticles. The EDS results suggested that the dyes biosorption onto microparticles occurred mainly by physical interactions, and for the nanoparticles, chemisorption was dominant.

1. Introduction

Many industries, such as, textile, food, cosmetics, pharmaceutical and others, use dyes to color their products and thus produce wastewater-containing organics with a strong color [1]. Due its low fixation degree, a large amount of these dyes are discharged into industrial effluents [2]. Dyes have become one of the main sources of severe water pollution, causing risks to the human health and aquatic biota [3]. Thus, several governments have established environmental restrictions with regard to the quality of colored wastewater and this obligated the industries to remove dyes from their effluents before discharging [4]. Dye wastewater is usually treated by flocculation combined with flotation, electroflocculation, membrane filtration, electrokinetic coagulation, electrochemical destruction, ion-exchange, irradiation, precipitation, ozonation, and katox treatment method involving the use of activated carbon and air mixtures. However, these technologies are generally ineffective in color removal, expensive and less adaptable to a wide range of dye wastewaters [5]. In this context, biosorption has emerged as an alternative eco-friendly technology to dye removal from industrial effluents. Biosorption have significant advantages in comparison with conventional methods, especially from economical and environmental viewpoints [2,5–7].

Biosorption is the removal of pollutants from aqueous solutions using non-growing or dead microbial mass, thus allowing the recovery and/or environmentally acceptable disposal of the pollutants. This term is used to indicate a number of metabolism-independent processes (physical and chemical adsorption, electrostatic interaction, ion exchange, complexation, chelation, and microprecipitation) that occur essentially in the cell wall [6]. Many biosorbents were employed to removal pollutants from aqueous solutions by biosorption, such as, fungi, bacteria, chitosan, algae and peat [2,3,5,6]. The literature shows that some biosorbents were successfully employed to removal dyes from aqueous solutions, for example, *Chlorella vulgaris* [7], *Ulothrix* sp. [8], *Ananas comosus* leaf powder [9] and *Scolymus hispanicus* [10]. However, the *Spirulina platensis* biomass is commonly applied to metal removal, such as, cadmium, cooper, lead and nickel [11–13], and the studies about dye removal onto *S. platensis* are very limited.

S. platensis, a member of blue-green algae, is an alternative source of protein for human food and feed purposes. Other than protein, it involves polysaccharides, lipids, and vitamins within [14]. These contain a variety of functional groups such as carboxyl, hydroxyl, sulfate, phosphate and other charged groups [11–13] which can be responsible for dye binding. This microalgae have availability in large quantities, is largely cultivated throughout worldwide and relatively cheap for the biosorption process [15]. In addition, the nanobiotechnology enables the obtaining of micro and nanoparticles from *S. platensis* biomass [16], suggesting that studies should be realized to verify its potential as a biosorbent.

* Corresponding author. Tel.: +55 53 3233 8648; fax: +55 53 3233 8745.
E-mail addresses: guilherme_dotto@yahoo.com.br (G.L. Dotto), titoeq@gmail.com (T.R.S. Cadaval), dqmpinto@furg.br (L.A.A. Pinto).

1359-5113/$ – see front matter © 2012 Elsevier Ltd. All rights reserved.
http://dx.doi.org/10.1016/j.procbio.2012.04.029

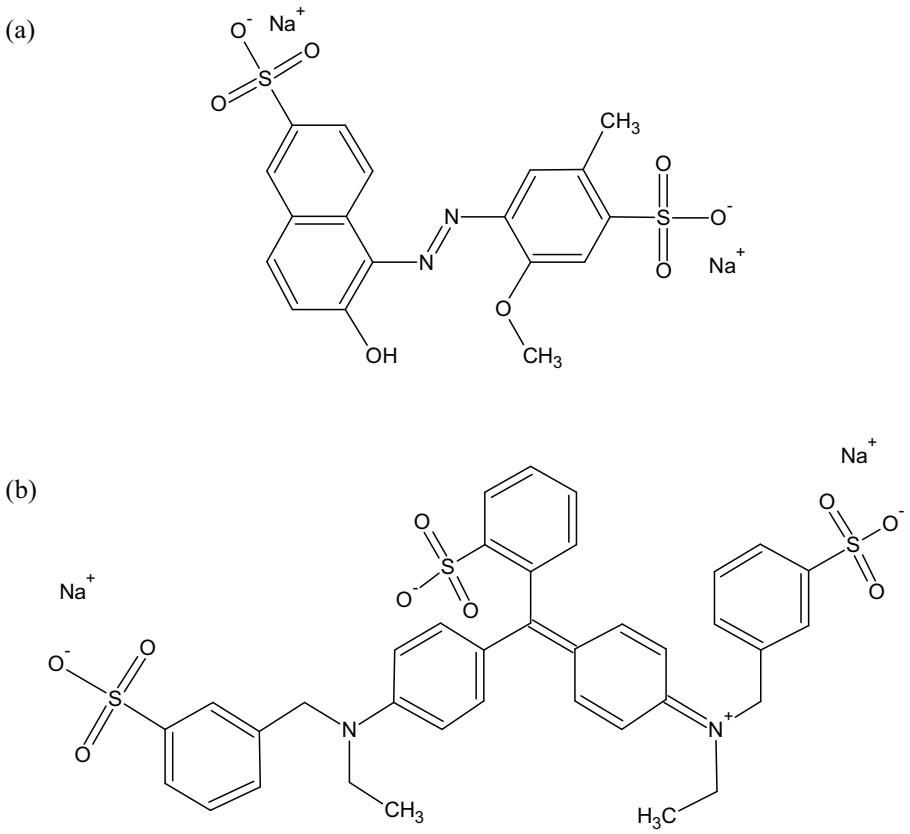

Fig. 1. Chemical structures of the dyes: (a) FD&C red no. 40; (b) acid blue 9.

The use of dead algal biomass in the form of a particulate material (micro and nanoparticles) to dyes removal is rarely investigated. In this work, the potential of micro and nanoparticles of *S. platensis* dead biomass as biosorbents to removal two synthetic dyes was investigated. The micro and nanoparticles were obtained and characterized by scanning electron microscopy (SEM), size distribution, specific surface area, pore volume and average pore radius (BET), infrared analysis (FTIR-ATR) and X-ray diffraction (XRD). The effects of particle size (micro and nano) and biosorbent dosage (from 50 to 750 mg) on biosorption capacity and percentage dye removal were studied. The models nominated pseudo-first order, pseudo-second order and Elovich were used to evaluate the biosorption kinetics. The energy dispersive X-ray spectroscopy (EDS) was employed to verify the biosorption nature.

2. Materials and methods

2.1. Dyes

The commercial synthetic dyes FD&C red no. 40 (azo dye, molecular weight 496.4 g mol^{-1}, C.I. 16,045, λ_{max} = 500 nm, pK_a = 11.4) and acid blue 9 (triphenylmethane dye, molecular weight 792.8 g mol^{-1}, C.I. 42,090, λ_{max} = 408 nm, pK_a 5.6 and 6.6) were supplied by local manufacturer, Plury Chemical Ltda., with a purity higher than 85%. All other utilized reagents were of analytical grade. Distilled water was used to prepare all solutions. The chemical structures of the dyes are illustrated in Fig. 1.

2.2. Culture conditions, drying and characterization of S. platensis biomass

S. platensis strain LEB-52 was cultivated in a 450 L open outdoor photobioreactors, under uncontrolled conditions, in the south of Brazil. During these cultivations, water was supplemented with 20% Zarrouk synthetic medium, containing (g L^{-1}): $NaHCO_3$, 16.8; $NaNO_3$, 2.5; K_2HPO_4, 0.5; K_2SO_4, 1.0; NaCl, 1.0; $MgSO_4{\cdot}7H_2O$, 0.2; $CaCl_2$, 0.04; $FeSO_4{\cdot}7H_2O$, 0.01; EDTA, 0.08 and micronutrients [14]. An initial biomass concentration was 0.15 g L^{-1}. Samples were taken at 24 h intervals and the biomass concentration determined by measuring the optical density of the cell suspension at 670 nm (Quimis, Q108, Brazil). A calibration curve was used to relate the optical density with the *S. platensis* biomass. At the end of cultivation, the biomass was recovered by filtration, washed and pressed to recover the biomass with a moisture content of 76% (wet basis).

The wet biomass (cylindrical pellet form with a diameter of 3 mm) was dried in perforated trays using perpendicular air flow. The drying conditions were: air temperature 60 °C, air velocity 1.5 m s^{-1}, relative humidity between 7 and 10%, tray load 4 kg m^{-2} [17].

The dried biomass was characterized according to the centesimal chemical composition [18], and elemental composition of the surface through energy dispersive X-ray spectroscopy (EDS) (Jeol, JSM-5800, Japan) [19].

2.3. Preparation and characterization of micro and nanoparticles

The microparticles were obtained as follows: the dried biomass of *S. platensis* was ground by a mill (Wiley Mill Standard, No. 03, USA) and it was sieved until the discrete particle size ranged from 68 to 75 μm. The size distribution and the average diameter of the microparticles were evaluated by a scanning electron microscope (SEM) (Jeol, JSM-6060, Japan). The identification, score and size measurement of the microparticles were carried out through the SEM micrographs by Image J software (NIH Image, USA) (analyze particle method) [20].

The nanoparticles were obtained from microparticles through a mechanical method [21]. The microparticles were added in distilled water (5 g L^{-1}) and pH was corrected (pH 3) using a buffer disodium phosphate/citric acid solution (0.1 mol L^{-1}). The suspension was agitated at 10,000 rpm (Dremel, 1100-01, Brazil) for 20 min. These conditions were obtained by preliminary tests. The size distribution and average diameter of the nanoparticles were determined in suspension through dynamic light scattering (DLS) [22]. This equipment was constituted by a laser (Spectra-physics, 127, USA) coupled to a goniometer (Brookheaven, BI-200M, USA) and a digital correlator (Brookheaven, BI-9000AT, USA).

The *S. platensis* micro and nano particles were characterized by scanning electron microscopy (SEM) (Jeol, JSM-6060, Japan) [20], point of zero charge (pH_{pzc}) (using the 11 points experiment [23]). The specific surface area, pore volume and average pore radius of the micro and nano particles were determined by standard BET N_2-adsorption methods (Quantachrome, Nova station A, USA) [8]. The identification of the functional groups was carried out using infrared analysis with attenuated total reflectance (FTIR-ATR) (Prestige 21, the 210045, Japan) [24]. X-ray diffraction (XRD) was carried out to verify the crystallinity or amorphous structure of the micro and nanoparticles [24].

2.4. Batch experiments

The *S. platensis* micro and nanoparticles (dosage of 50; 150; 250; 350; 450; 550; 650 and 750 mg) were added in 0.80 L of distilled water. The pH was corrected (pH 3) (Mars, MB10, Brazil) [15] with the 50 mL of buffer disodium phosphate/citric acid solution (0.1 mol L^{-1}), which did not present interaction with the dyes [25]. 50 mL of a solution containing 10 g L^{-1} of dyes was added to each *S. platensis* suspension, and it was completed to 1 L with distilled water, thus, the initial dye concentration was approximately 500 mg L^{-1} [5].

The experiments were carried out in a jar test (Nova etica, 218 MBD, Brazil), under agitation (400 rpm) [26] and ambient temperature (25 ± 1 °C) [7]. Aliquots were withdrawn in preset time intervals (2; 4; 6; 8; 10; 15; 20; 25; 30; 40; 50; 60; 80; 100; 120 min and at equilibrium (24 h)). The biomass and biosorbed dyes were removed of liquid through a filtration with Whatmann filter paper no. 40, which did not present interaction with the dyes [25,26], and the dyes concentration was determined by spectrophotometry (Quimis, Q108, Brazil). All experiments were carried out in replicate and blanks were performed.

The biosorption capacities at time t (q_t) and at equilibrium (q_e), and the percentage dye removal (R) were determined as follows:

$$q_t = \frac{C_0 - C_t}{m} V \quad (1)$$

$$q_e = \frac{C_0 - C_e}{m} V \quad (2)$$

$$R(\%) = \frac{C_0 - C_e}{C_0} \times 100 \quad (3)$$

where C_0 is the initial dye concentration in liquid phase (mg L^{-1}), C_t is the dye concentration in liquid phase at time t (mg L^{-1}), C_e is the dye concentration in liquid phase at equilibrium (mg L^{-1}), m is biosorbent dosage (g) and V is the volume of suspension (L).

2.5. Kinetic models

Biosorption kinetics is important design parameter that describes how the adsorbate interacts with the biosorbent [6,7,15,26–28]. It was investigated by fit of the experimental data to the models of pseudo-first order, pseudo-second order and Elovich.

The kinetic models of pseudo-first order [29] and pseudo-second order [30] assume that adsorption is a pseudo-chemical reaction, and the adsorption rate can be determined, respectively, for equations of pseudo-first and pseudo-second order, as follows:

$$q_t = q_1(1 - \exp(-k_1 t)) \quad (4)$$

$$q_t = \frac{t}{(1/k_2 q_2^2) + (t/q_2)} \quad (5)$$

where q_t is the adsorbate amount adsorbed at time t (mg g^{-1}), k_1 and k_2 are the rate constants of pseudo-first and pseudo-second order models, respectively, in (min^{-1}) and (g mg^{-1} min^{-1}), q_1 and q_2 are the theoretical values for the adsorption capacity (mg g^{-1}) and t is the time (min).

When the adsorption processes occurs through chemisorption in solid surface, and the adsorption velocity decreases with time due to covering of the superficial layer, the Elovich model is most used. The Elovich kinetic model is described as follows [31]:

$$q_t = \frac{1}{a} \ln(1 + abt) \quad (6)$$

where "a" is the initial velocity due to dq/dt with $q_t = 0$ (mg g^{-1} min^{-1}) and "b" is the desorption constant of the Elovich model (g mg^{-1}).

The coefficients values of the kinetic equations were determined from fit of the models to the experimental data by nonlinear regression, using Statistic 7.0 software (Statsoft, USA) through Quasi-Newton estimation method. The fit quality was measured through coefficients of determination (R^2) and average relative error (ARE) [26].

2.6. Biosorption nature

In order to elucidate the biosorption nature of the micro and nanoparticles, the analyses of energy dispersive spectroscopy (EDS) (Jeol, JSM-5800, Japan) [19,27] were performed before and after the biosorption process.

3. Results and discussion

3.1. S. platensis biomass characterization

The centesimal chemical and elemental compositions of *S. platensis* dried biomass were showed in Table 1. Similar centesimal chemical composition was found by Oliveira et al. [17].

Table 1
Centesimal chemical composition and elemental composition of *Spirulina platensis* dried biomass.

Centesimal composition	(%, wet basis)[a]
Moisture content	9.0 ± 0.5
Ash	7.0 ± 0.2
Protein	67.2 ± 0.7
Lipids	7.5 ± 0.1
Carbohydrate[b]	9.8 ± 0.5
Elemental composition	**(%)[c]**
C	54.1 ± 0.5
N	33.1 ± 0.2
O	9.8 ± 0.1
P	1.8 ± 0.1
S	1.2 ± 0.1

[a] Mean values ± standard error in triplicate.
[b] By difference.
[c] Mean values ± standard error obtained from EDS analysis of five surfaces of the dried biomass.

It can be observed in Table 1 that the *S. platensis* biomass is composed by a variety of biomacromolecules and its major elements on the surface were C, N, O, P and S. These biomacromolecules contain a variety of functional groups such as carboxyl, hydroxyl, sulfate, phosphate, aldehydes, ketones and other charged groups [11–13,15], suggesting that the *S. platensis* microalgae can be considered an alternative to dye removal.

3.2. Micro and nanoparticles characterization

3.2.1. SEM images

The SEM images of *S. platensis* micro and nanoparticles are shown in Fig. 2(a) and (b), respectively. As can be seen in Fig. 2(a) and (b), the micro and nano particles are homogeneous with a uniform distribution. The microparticles presented different forms (Fig. 2(a)), while the nanoparticles presented an ellipsoidal-spherical form (Fig. 2(b)).

3.2.2. Size distribution and average diameter

Fig. 3(a) shows the size distribution of the *S. platensis* microparticles (obtained from SEM using Image J software). Fig. 3(b) shows the size distribution of the *S. platensis* nanoparticles (obtained from dynamic light scattering (DLS)).

In Fig. 3(a) it can be observed that *S. platensis* microparticles showed a normal and uniform size distribution in the range from 68 to 75 μm (according shown in Fig. 2(a)). The average diameter of the microparticles was 72 μm. In the same way, Fig. 3(b) shows that the *S. platensis* nanoparticles presented a normal and uniform size distribution. In this figure the nanoparticles in suspension showed range from 120 to 350 nm (according to Fig. 2(b)), and the average diameter was 215 nm. Nanoparticles are commonly described as solid colloidal particles, ranging in size from 10 nm to 1 μm [16,20,21]. In addition DLS showed that the autocorrelation function was unimodal (figure not shown) and the polydispersity index was 0.152, confirming a low variation in the nanoparticles size.

3.2.3. Point of zero charge (pH_{ZPC})

The 11 points experiment showed that the pH_{zpc} of the *S. platensis* micro and nanoparticles was 7. When the pH of the suspension is lower than 7, the surface of the *S. platensis* gets positively charged, and the surface of the *S. platensis* is negatively charged in pH values higher than 7. The zero point charge (pH_{zpc}) of the biosorbent is one way to understand the biosorption mechanisms [12,23].

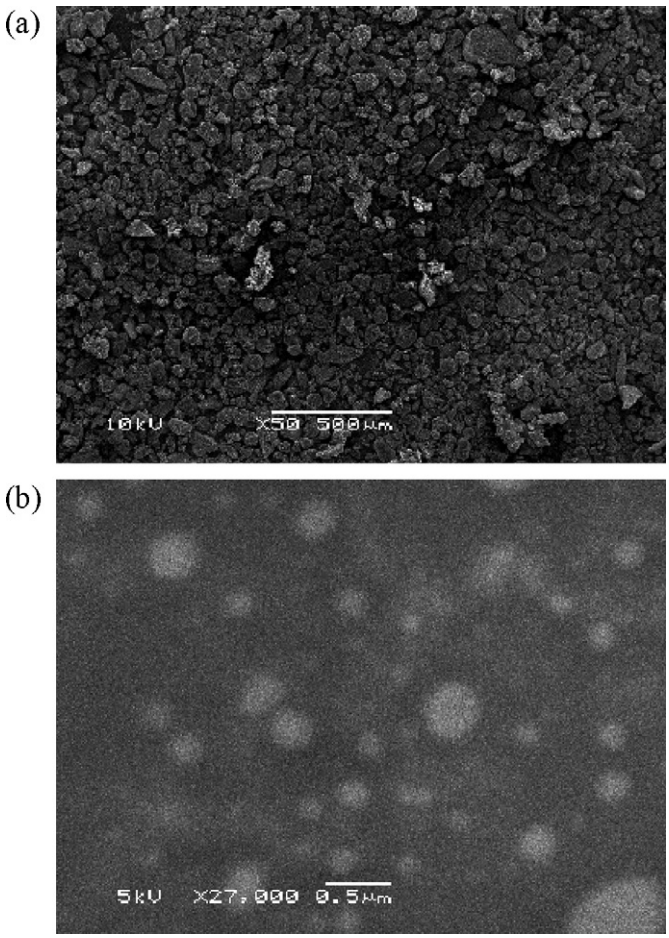

Fig. 2. SEM images of *Spirulina platensis*: (a) microparticles; (b) nanoparticles.

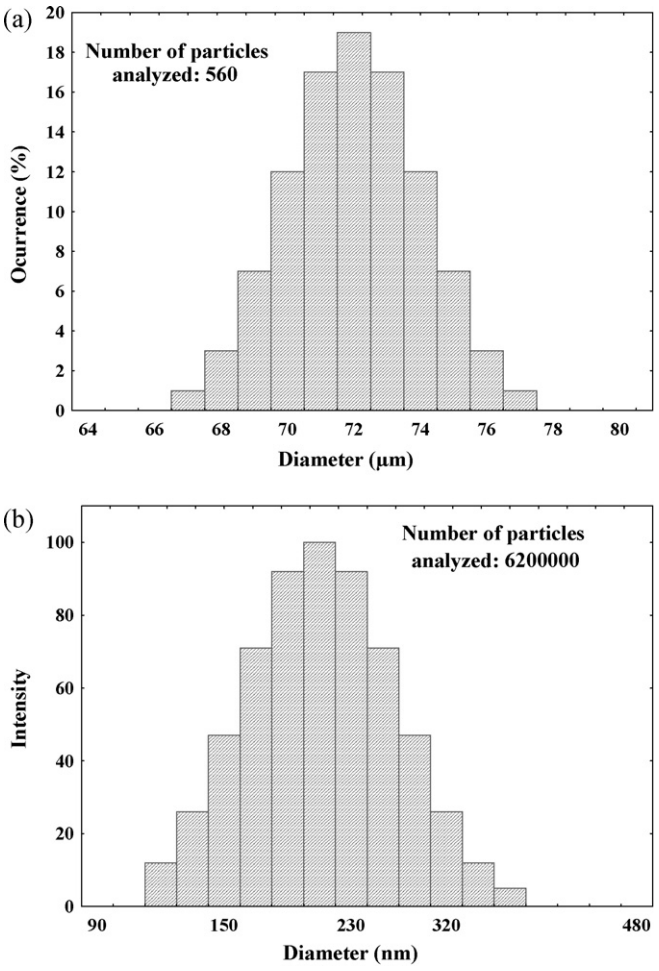

Fig. 3. Size distribution of *Spirulina platensis*: (a) microparticles (from SEM); (b) nanoparticles (from DLS).

3.2.4. Specific surface area, pore volume and average pore radius

The values of specific surface area, pore volume and average pore radius of the micro and nanoparticles are shown in Table 2.

It was observed in Table 2 that the average diameter decrease from 72 μm (microparticles) to 215 nm (nanoparticles) caused an increase of four times in the specific surface area, and about 55% in the pore volume. However, the average pore radius was not modified (Table 2). This suggests that the high stirring used to obtain the nanoparticles (10,000 rpm) caused an improvement in the biosorption characteristics of *S. platensis*.

3.2.5. FTIR-ATR analysis

Fig. 4 shows the FTIR-ATR spectrum of *S. platensis* for microparticles and nanoparticles.

For the microparticles, the major intense bands were: 3282, 2926, 2852, 1650, 1549, 1458, 1419 and 1030 cm^{-1} (Fig. 4(a)). The peak at 3282 cm^{-1} is relative to the O—H and N—H stretching. The asymmetric and symmetric stretching of CH_2 can be observed at 2926 and 2852 cm^{-1}, respectively. At 1650 cm^{-1} the C=C stretch was observed. The interaction N—H bending with C—N stretching can be observed at 1549 cm^{-1}. The bending of NH^{4+} was identified at 1458 cm^{-1}. The peak at 1419 cm^{-1} is relative to the C—N stretching of primary amide. The P—O links were observed at 1030 and 1080 cm^{-1}.

In Fig. 4(b) (nanoparticles) the same peaks of microparticles were maintained (3356, 3284, 2922, 2852, 1651, 1556, 1543, 1458, 1419, 1084, 1028 cm^{-1}) and some new peaks were observed (1635, 1622, 1388, 1151 and 972 cm^{-1}). The scissor bending of primary amine appeared at 1635 and 1622 cm^{-1}. The aldehydes and ketones groups can be observed at 1388 and 1151 cm^{-1}, respectively. The S—O stretching was identified at 972 cm^{-1}. In addition, for the nanoparticles the transmittance values were lower in relation to the microparticles, consequently, the absorbance values were higher, and more energy was necessary to generate the peaks in the spectrum of the nanoparticles. This shows that the nanoparticles contain more accessible sites for dye binding in relation to the microparticles.

The differences between Fig. 4(a) (spectrum of the microparticles) and Fig. 4(b) (spectrum of the nanoparticles) occurred because during the preparation of the nanoparticles, the high-energy dissipation caused an exposure of more functional groups.

Table 2
Characteristics of *Spirulina platensis* micro and nano particles: specific surface area, pore volume and average pore radius.

Particle characteristic	Microparticles (72 μm)	Nanoparticles (215 nm)
Specific surface area ($m^2\ g^{-1}$)[a]	3.5 ± 0.1	14.2 ± 0.1
Pore volume ($mm^3\ g^{-1}$)[a]	3.9 ± 0.2	6.9 ± 0.1
Average pore radius (Å)[a]	22.5 ± 0.5	22.6 ± 0.3

[a] Mean values ± standard error in triplicate.

3.2.6. XRD patterns

In Fig. 5 are shown the XRD patterns of the microparticles and nanoparticles.

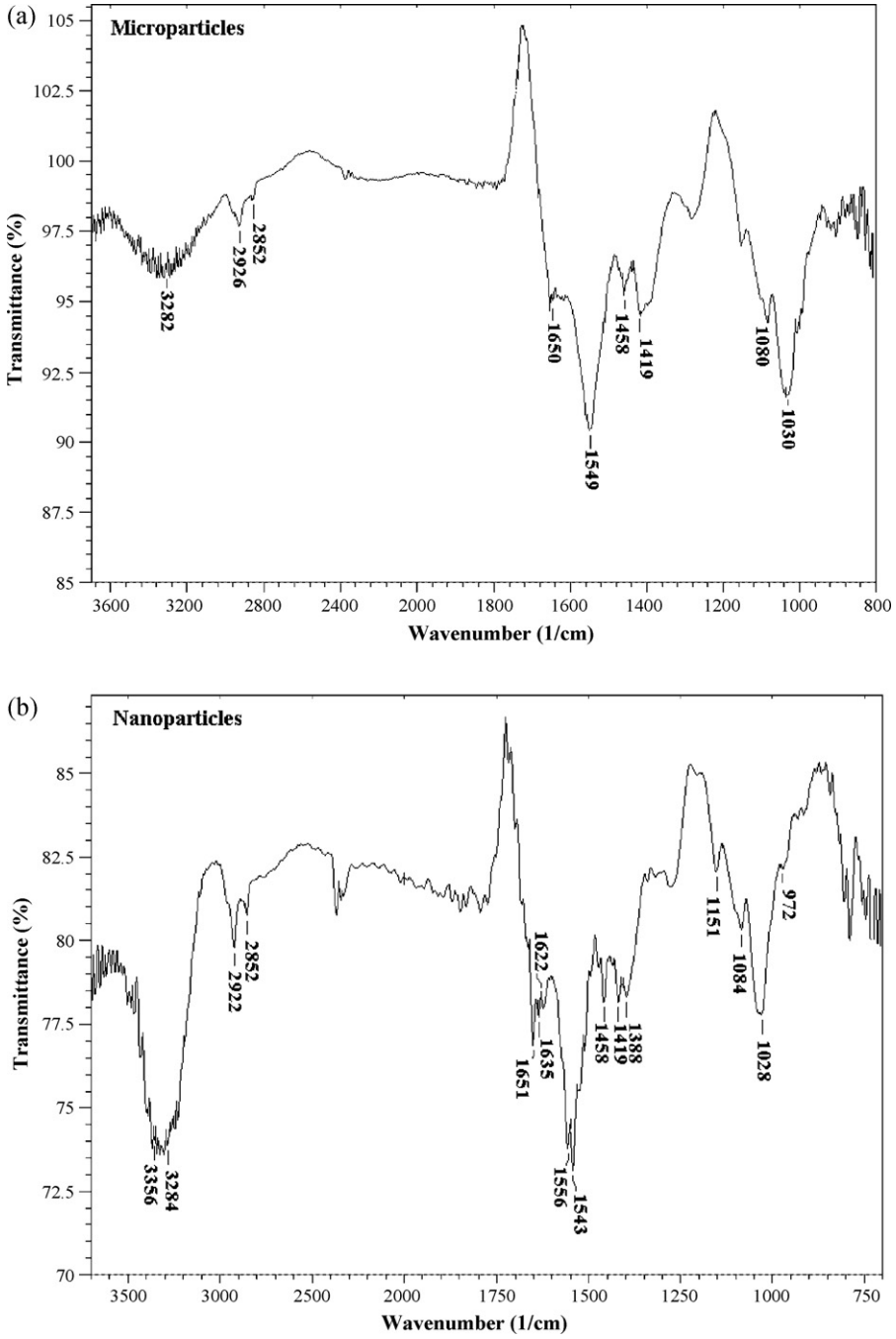

Fig. 4. FTIR-ATR spectrum of *S. platensis*: (a) microparticles; (b) nanoparticles.

The XRD pattern of the microparticles (Fig. 5(a)) indicates a shape of typical amorphous in nature, but some crystalline zones were observed. On the other hand, the nanoparticles (Fig. 5(b)) showed a totally amorphous character. This shows that during the preparation of the nanoparticles, the *S. platensis* structure was modified, and the crystalline zones disappeared.

3.3. Particle size and biosorbent dosage effects

The effects of particle size and biosorbent dosage on dyes biosorption are shown in Fig. 6 (FD&C red no. 40) and Fig. 7 (acid blue 9).

It can be observed in Figs. 6 and 7 that the biosorption capacity and percentage dye removal values were increased when nanoparticles were used (Figs. 6(b) and 7(b)). This occurred because during the preparation of the nanoparticles, a very high stirring was employed (10,000 rpm), leading to the break of the microparticles. As consequence, occurred an increase in the surface area and pore volume (Table 2) and more biosorption sites on the surface were accessible for dye binding (Fig. 4(b)). In addition, the totally amorphous character (Fig. 5(b)) can be facilitates the dyes biosorption. According to Aksu [6] the biosorption is related directly with surface area of biosorbent, so particle size is also one of the important factors which affect the biosorption capacity. Similar behavior was found by Chu and Chen [32] in the biosorption of basic yellow 24 using dried activated sludge biomass. This situation was explained by larger total surface area of smaller particles, for the same amount of biomass.

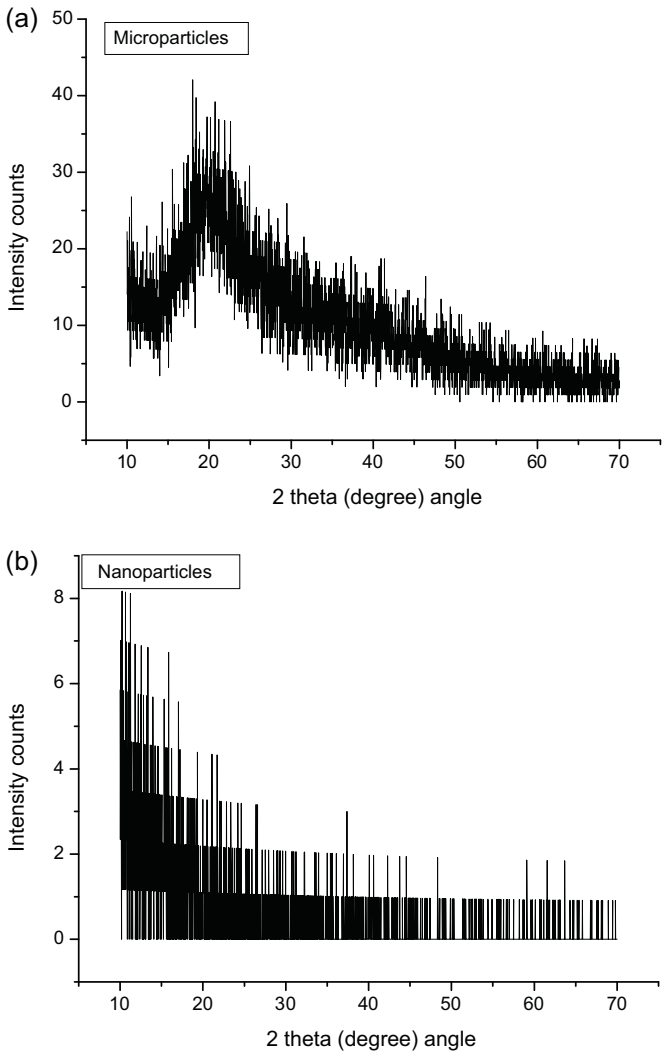

Fig. 5. X-ray diffraction patterns of *S. platensis*: (a) microparticles; (b) nanoparticles.

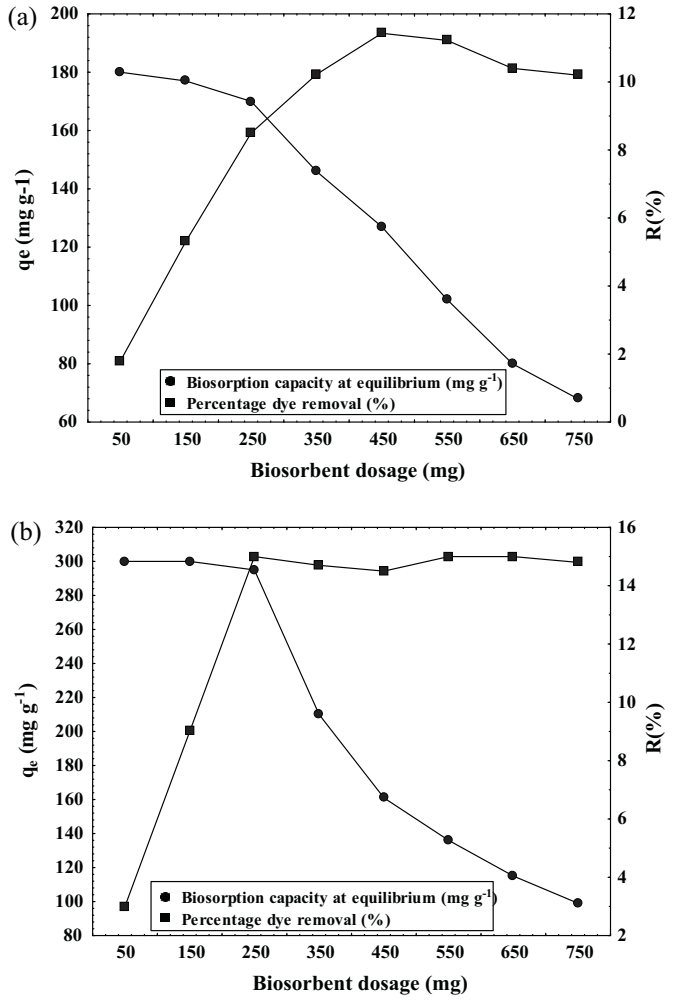

Fig. 6. Biosorbent dosage effect on biosorption of FD&C red no. 40: (a) microparticles; (b) nanoparticles.

It was observed in Figs. 6 and 7, that the percentage dye removal was increased with the increase of biosorbent dosage until 250 mg. After this value, the percentage dye removal was little influenced. According to Chowdhury et al. [9] the positive correlation between the biosorbent dosage and dye removal can be related to increased biosorbent surface area and availability of more sorption sites. In addition, Figs. 6 and 7 showed that the use of biosorbent dosages higher than 250 mg leads to a large decrease in the biosorption capacity. These results suggest that under experimental conditions, the use of 250 mg was the more appropriate in relation to the biosorption capacity and percentage dye removal.

The comparison between Figs. 6 and 7 shows that the biosorption capacity of FD&C red no. 40 was lower than acid blue 9. This fact can be explained based in the interaction mechanism. Under acidic conditions, the *S. platensis* surface is positively charged ($pH_{ZPC} = 7$) and the dyes dissociate in the anionic form (D-SO_3—). In this way, electrostatic interactions between the dyes sulfonated groups and *S. platensis* surface (positively charged) occurred [33,34]. The acid blue 9 pK_a (5.6 and 6.6) is lower than FD&C red no. 40 pK_a (11.4), facilitating the dissociation of D-SO_3Na and its conversion to D-SO_3—. In addition, acid blue 9 had more sulfonated groups than FD&C red no. 40 (Fig. 1). This manner, the interactions between *S. platensis* and acid blue 9 were facilitated, leading to higher values of biosorption capacity. Some researches demonstrated that the sulfonated groups of the anionic dyes are responsible to the dye–biosorbent interactions [3,6,25–28].

In summary, these results demonstrate that for the biosorption of both dyes, the nanoparticles were superior in relation to the microparticles. This occurred because nanoparticles presented more appropriate characteristics, such as, surface area, pore volume, biosorption accessible sites and totally amorphous character than microparticles. The more appropriate condition for the removal both dyes was 250 mg of nanoparticles. In these conditions the biosorption capacities were 295 mg g^{-1} and 1450 mg g^{-1}, and the percentage removal were 15.0 and 72.5%, for the FD&C red no. 40 and acid blue 9, respectively. Biosorption capacities of 555.6 mg g^{-1}, 196.1 mg g^{-1} and 71.9 mg g^{-1} were found by Aksu and Tezer [7] in the biosorption of reactive dyes on the green alga *C. vulgaris*. Dogar et al. [8] obtained biosorption capacity of 86.1 mg g^{-1} in the removal of methylene blue using green algae *Ulothrix* sp.

3.4. Biosorption kinetics

The biosorption kinetics was carried out using 250 mg of micro and nanoparticles. The kinetic curves of FD&C red no. 40 and acid blue 9 biosorption onto *S. platensis* micro and nanoparticles are shown in Fig. 8(a) and (b), respectively.

Fig. 8 shows that, in the case of the microparticles, similar behavior was observed for both dyes. Biosorption was fast, reaching about

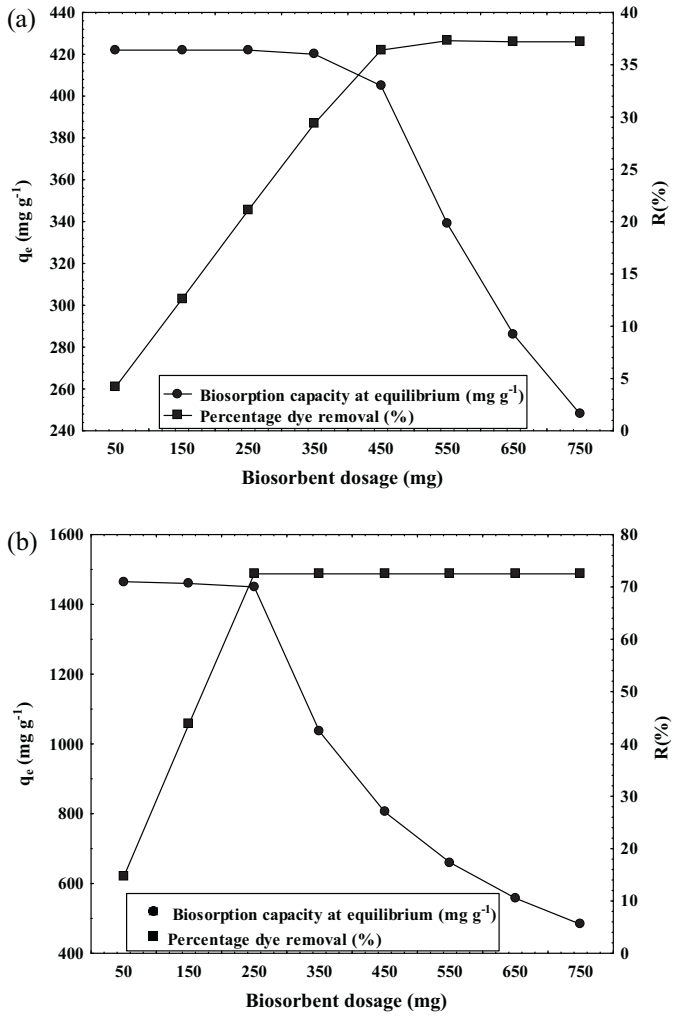

Fig. 7. Biosorbent dosage effect on biosorption of acid blue 9: (a) microparticles; (b) nanoparticles.

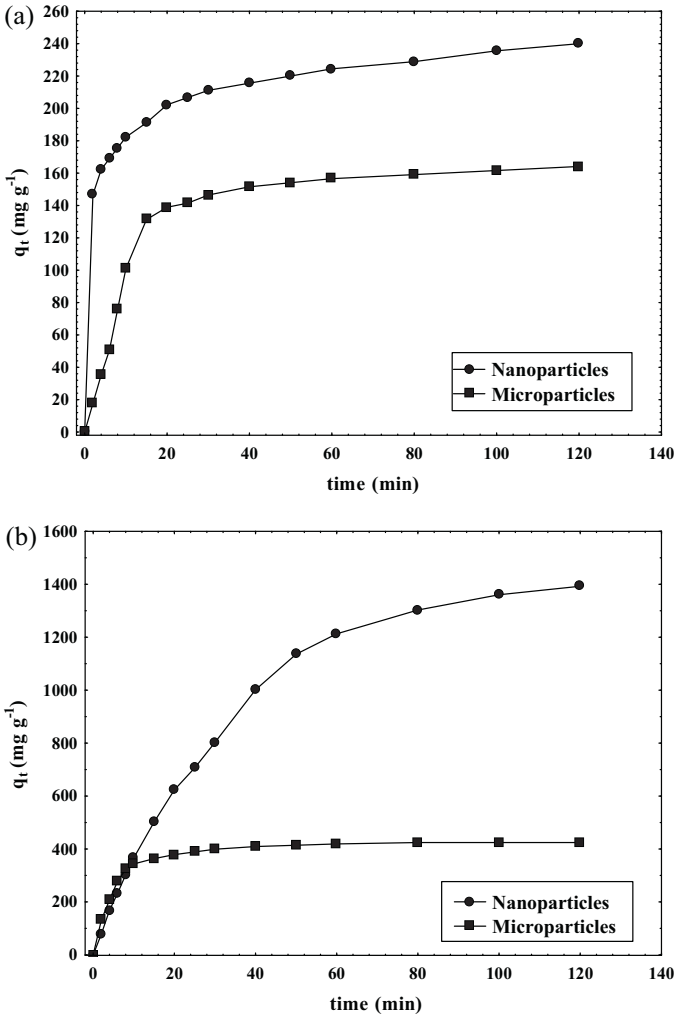

Fig. 8. Biosorption kinetics onto *Spirulina platensis* micro and nanoparticles (dosage 250 mg): (a) FD&C red no. 40; (b) acid blue 9.

90% of saturation during the first 20 min. Later, biosorption rate decreased considerably. On the other hand, for the nanoparticles about 90% of saturation was reached at 50 min for the FD&C red no. 40, and at 80 min for the acid blue 9. These results show that the biosorption onto microparticles was faster than the nanoparticles, however, the nanoparticles presented higher values of biosorption capacity. This occurred because during the biosorption process, the accessible biosorption sites on the surface of micro and nanoparticles were progressively blocked by the dyes, and the nanoparticles had more accessible biosorption sites on the surface in relation to microparticles (Fig. 4). As consequence, the microparticles reached the dynamic equilibrium more rapidly and its biosorption capacity was lower. Similar behavior was found by Annadurai et al. [35] in the adsorption of remazol black 13 onto chitosan. Their results showed that the increase in particle size caused an increase in the adsorption rate, but lower values of adsorption capacity were obtained.

In order to evaluate the biosorption kinetics, pseudo-first order, pseudo-second order and Elovich models were fitted to the experimental data. The kinetic parameters of FD&C red no. 40 and acid blue 9 biosorption onto *S. platensis* micro and nanoparticles are shown in Table 3.

The high values of coefficient of determination ($R^2 = 0.999$) and the low values of average relative error (ARE < 5.0%) presented in Table 3 shows that the Elovich model was the best to represent the biosorption of both dyes onto nanoparticles. According to some researchers, the Elovich equation describes chemisorption (chemical reaction) mechanism in nature [26–28,31]. This shows that the chemisorption played an important role in the biosorption of both dyes onto *S. platensis* nanoparticles, and the nanoparticles were covered by superficial layer of the dyes [31]. However, pseudo-first order was more adequate to represent the biosorption onto microparticles ($R^2 > 0.98$ and ARE < 10.0%). This shows that the biosorption of both dyes onto microparticles was a very fast process. In addition, the chemisorption was not dominant in this case because the Elovich and pseudo-second order models showed no satisfactory fit [6,7,26–28].

3.5. Biosorption nature

Energy dispersive spectroscopy analyses (EDS) were employed to elucidate the biosorption of both dyes onto micro and nanoparticles. The data of EDS elemental analysis of micro and nanoparticles before and after biosorption are shown in Table 4.

It can be observed in Table 4 that the major elements on the surface of the microparticles before biosorption were C, N, O, P and S. After the biosorption process, no changes in the percentages of these elements were observed. This shows that the biosorption onto microparticles occurred by weak interactions. According to Aksu [6], weak interactions are characteristic of

Table 3
Biosorption kinetic parameters of FD&C red no. 40 and acid blue 9 onto *Spirulina platensis* micro and nanoparticles (Biosorbent dosage 250 mg).

Kinetic models	FD&C red no. 40[a]		Acid blue 9[a]	
	Microparticles	Nanoparticles	Microparticles	Nanoparticles
Pseudo-first order				
q_1 (mg g^{-1})	160.6 ± 1.1	212.6 ± 2.3	410.6 ± 2.1	1453.7 ± 3.6
k_1 (min^{-1})	0.08 ± 0.01	0.37 ± 0.02	0.18 ± 0.01	0.03 ± 0.01
R^2	0.983	0.892	0.991	0.968
ARE (%)	9.1	8.3	2.9	2.3
Pseudo-second order				
q_2 (mg g^{-1})	185.8 ± 2.0	226.4 ± 1.5	447.4 ± 1.2	1358.4 ± 3.5
$k_2 \times 10^4$ (g mg^{-1} min^{-1})	5.4 ± 0.1	26.7 ± 1.2	5.9 ± 0.2	0.4 ± 0.1
R^2	0.961	0.966	0.961	0.927
ARE (%)	14.7	4.6	5.3	25.3
Elovich				
$a \times 10^2$ (mg g^{-1} min^{-1})	2.51 ± 0.15	4.32 ± 0.07	1.51 ± 0.02	0.17 ± 0.03
b (g mg^{-1})	34.2 ± 1.8	6316.0 ± 10.1	663.9 ± 3.1	57.3 ± 2.7
R^2	0.909	0.999	0.926	0.999
ARE (%)	22.1	0.7	10.0	4.7

[a] Mean values ± standard error (n = 3).

Table 4
Elemental composition of *Spirulina platensis* micro and nanoparticles before and after dye biosorption.

	Elements (%)[a]				
	C	N	O	P	S
Microparticles					
Before biosorption	55.7 ± 1.4	32.6 ± 1.5	9.1 ± 0.5	1.5 ± 0.1	1.1 ± 0.1
After FD&C red no. 40 biosorption	54.7 ± 1.7	33.5 ± 0.7	9.0 ± 0.5	1.4 ± 0.1	1.4 ± 0.5
After acid blue 9 biosorption	55.0 ± 0.9	32.7 ± 0.7	10.0 ± 2.0	1.4 ± 0.1	0.9 ± 0.1
Nanoparticles					
Before biosorption	54.2 ± 0.9	33.7 ± 0.3	9.1 ± 0.4	1.7 ± 0.1	1.3 ± 0.1
After FD&C red no. 40 biosorption	58.8 ± 0.7	24.3 ± 0.5	13.3 ± 0.2	0.5 ± 0.1	3.1 ± 0.1
After acid blue 9 biosorption	67.1 ± 0.5	15.8 ± 0.5	12.3 ± 0.2	0.6 ± 0.1	4.2 ± 0.1

[a] Mean values ± standard error obtained from EDS analysis of five surfaces of samples.

physical interactions and responsible for lower values of biosorption capacity. In addition, in physical biosorption, equilibrium is usually rapidly attained and easily reversible [6], confirming thus the biosorption kinetic behavior of both dyes onto microparticles.

For the nanoparticles before biosorption, the major elements on the surface were C, N, O, P and S (Table 4). After biosorption, the percentages of C, O, and S were increased, and consequently, the percentages of N and P were decreased. This occurred due to the trapped dye molecules which contain aromatic rings and sulfonic groups, indicating strong interaction between dyes and nanoparticles. According to Aksu [6], strong interactions are characteristic of chemical interactions and responsible for higher values of biosorption capacity.

4. Conclusion

The potential of *S. platensis* micro and nanoparticles as biosorbents to removal FD&C red no. 40 and acid blue 9 synthetic dyes was investigated. The best results for both dyes were found using 250 mg of nanoparticles. In these conditions, the biosorption capacities were 295 mg g^{-1} and 1450 mg g^{-1}, and the percentages of dye removal were 15.0 and 72.5%, for the FD&C red no. 40 and acid blue 9, respectively. This manner, *S. platensis* nanoparticles can be considered to dye removal from aqueous solutions, mainly the acid blue 9 dye. The kinetic study showed that the biosorption onto microparticles was faster than biosorption onto nanoparticles, however, nanoparticles presented biosorption capacities higher than microparticles. Pseudo-first order model was the best to represent biosorption of both dyes onto microparticles (R^2 > 0.98 and ARE < 10%), and Elovich model was more appropriate to the biosorption onto nanoparticles (R^2 > 0.99 and ARE < 5%). The kinetic results coupled by the EDS analysis suggested that the dyes biosorption onto microparticles occurred by physical interactions and for the nanoparticles, chemisorption was dominant.

Acknowledgements

The authors would like to thank CAPES (Brazilian Agency for Improvement of Graduate Personnel) and CNPq (National Council of Science and Technological Development) for the financial support.

References

[1] Salleh MAM, Mahmoud DK, Karim WAWA, Idris A. Cationic and anionic dye adsorption by agricultural solid wastes: a comprehensive review. Desalination 2011;280:1–13.
[2] Gupta VK, Suhas. Application of low-cost adsorbents for dye removal: a review. J Environ Manage 2009;90:2313–42.
[3] Wan Ngah WS, Teong LC, Hanafiah MAKM. Adsorption of dyes and heavy metal ions by chitosan composites: a review. Carbohydr Polym 2011;83:1446–56.
[4] Mahmoodi NM, Hayati B, Arami M. Single and binary system dye removal from colored textile wastewater by a dendrimer as a polymeric nanoarchitecture: equilibrium and kinetics. J Chem Eng Data 2010;55:4660–8.
[5] Srinivasan A, Viraraghavan T. Decolorization of dye wastewaters by biosorbents: a review. J Environ Manage 2010;91:1915–29.
[6] Aksu Z. Application of biosorption for the removal of organic pollutants: a review. Proc Biochem 2005;40:997–1026.
[7] Aksu Z, Tezer S. Biosorption of reactive dyes on the green alga *Chlorella vulgaris*. Proc Biochem 2005;40:1347–61.
[8] Dogar Ç, Gurses A, Açıkyıldız M, Ozkan E. Thermodynamics and kinetic studies of biosorption of a basic dye from aqueous solution using green algae *Ulothrix* sp. Colloids Surf B: Biointerfaces 2010;76:279–85.
[9] Chowdhury S, Chakraborty S, Saha P. Biosorption of Basic Green 4 from aqueous solution by *Ananas comosus* (pineapple) leaf powder. Colloids Surf B: Biointerfaces 2011;84:520–7.

[10] Barka N, Abdennouri M, El Makhfouk M. Removal of methylene blue and Eriochrome black T from aqueous solutions by biosorption on *Scolymus hispanicus* L.: kinetics, equilibrium and thermodynamics. J Taiwan Inst Chem Eng 2011;42:320–6.
[11] Seker A, Shahwan T, Eroglu A, Yılmaz S, Demirel Z, Dalay M. Equilibrium, thermodynamic and kinetic studies for the biosorption of aqueous lead(II), cadmium(II) and nickel(II) ions on *Spirulina platensis*. J Hazard Mater 2008;154:973–80.
[12] Çelekli A, Bozkurt H. Bio-sorption of cadmium and nickel ions using *Spirulina platensis*: kinetic and equilibrium studies. Desalination 2011;275:141–7.
[13] Fang L, Zhou C, Cai P, Chen W, Rong X, Dai K, et al. Binding characteristics of copper and cadmium by cyanobacterium *Spirulina platensis*. J Hazard Mater 2011;190:810–5.
[14] Costa JAV, Colla LM, Duarte PFF. Improving *Spirulina platensis* biomass yield using a fed-batch process. Bioresour Technol 2004;92:237–41.
[15] Çelekli A, Yavuzatmac M, Bozkurt H. An eco-friendly process: predictive modelling of copper adsorption from aqueous solution on *Spirulina platensis*. J Hazard Mater 2010;173:123–9.
[16] Anton N, Benoit JP, Saulnier P. Design and production of nanoparticles formulated from nano-emulsion templates—a review. J Control Release 2008;128:185–99.
[17] Oliveira EG, Rosa GS, Moraes MA, Pinto LAA. Characterization of thin layer drying of *Spirulina platensis* utilizing perpendicular air flow. Bioresour Technol 2009;100:1297–303.
[18] AOAC. Official methods of analysis. 14 ed. Washington, DC: AOAC; 1995.
[19] Sadri S, Moghaddam MR, Moghaddam A, Arami M. Coagulation/flocculation process for dye removal using sludge from water treatment plant: optimization through response surface methodology. J Hazard Mater 2010;175:651–7.
[20] Li X, Anton N, Arpagaus C, Belleteix F, Vandamme TF. Nanoparticles by spray drying using innovative new technology: the Büchi Nano Spray Dryer B-90. J Control Release 2010;147:304–10.
[21] Anton N, Benoit JP, Saulnier P. Design and production of nanoparticles formulated from nano-emulsion templates: a review. J Control Release 2008;128:185–99.
[22] Bruce J, Pecora R. Dynamic light scattering: with applications to chemistry, biology, and physics. New York: Dover publications; 2000.
[23] Hao X, Quach L, Korah J, Spieker WA, Regalbuto JR. The control of platinum impregnation by PZC alteration of oxides and carbon. J Mol Catal A: Chem 2004;219:97–107.
[24] Muzzarelli C, Stanic V, Gobbi L, Tosi G, Muzzarelli RAA. Spray-drying of solutions containing chitosan together with polyuronans and characterisation of the microspheres. Carbohydr Polym 2004;57:73–82.
[25] Piccin JS, Vieira MLG, Gonçalves JO, Dotto GL, Pinto LAA. Adsorption of FD&C red no 40 by chitosan: isotherms analysis. J Food Eng 2009;95:16–20.
[26] Dotto GL, Pinto LAA. Adsorption of food dyes acid blue 9 and food yellow 3 onto chitosan: stirring rate effect in kinetics and mechanism. J Hazard Mater 2011;187:164–70.
[27] Dotto GL, Pinto LAA. Adsorption of food dyes onto chitosan: optimization process and kinetic. Carbohydr Polym 2011;84:231–8.
[28] Piccin JS, Dotto GL, Vieira MLG, Pinto LAA. Kinetics and mechanism of the food dye FD&C red no 40 adsorption onto chitosan. J Chem Eng Data 2011;56:3759–65.
[29] Lagergren S. About the theory of so-called adsorption of soluble substances. Kung Svenska Vetenskaps 1898;24:1–39.
[30] Ho YS, McKay G. Pseudo-second order model for sorption processes. Process Biochem 1999;34:451–65.
[31] Wu FC, Tseng RL, Juang RS. Characteristics of Elovich equation used for the analysis of adsorption kinetics in dye chitosan systems. Chem Eng J 2009;150:366–73.
[32] Chu CH, Chen KM. Reuse of activated sludge biomass: II. The rate processes for the adsorption of basic dyes on biomass. Proc Biochem 2002;37:1129–34.
[33] Dotto GL, Lima EC, Pinto LAA. Biosorption of food dyes onto *Spirulina platensis* nanoparticles: equilibrium isotherm and thermodynamic analysis. Bioresour Technol 2012;103:123–30.
[34] Dotto GL, Esquerdo VM, Vieira MLG, Pinto LAA. Optimization and kinetic analysis of food dyes biosorption by *Spirulina platensis*. Colloids Surf B: Biointerfaces 2012;91:234–41.
[35] Annadurai G, Ling LY, Lee JF. Adsorption of reactive dye from an aqueous solution by chitosan: isotherm, kinetic and thermodynamic analysis. J Hazard Mater 2008;152:337–46.